




Hund electronic correlation in $\text{La}_3\text{Ni}_2\text{O}_7$ under high pressure

Zhenfeng Ouyang ^{1,2}, Jia-Ming Wang,^{1,2} Jing-Xuan Wang,^{1,2} Rong-Qiang He ^{1,2,*}, Li Huang,^{3,†} and Zhong-Yi Lu ^{1,2,‡}

¹*Department of Physics and Beijing Key Laboratory of Opto-Electronic Functional Materials and Micro-Nano Devices, Renmin University of China, Beijing 100872, China*

²*Key Laboratory of Quantum State Construction and Manipulation, Ministry of Education, Renmin University of China, Beijing 100872, China*

³*Science and Technology on Surface Physics and Chemistry Laboratory, P.O. Box 9-35, Jianguo 621908, China*



(Received 24 November 2023; revised 19 January 2024; accepted 16 February 2024; published 11 March 2024)

By means of density functional theory plus dynamical mean-field theory, we investigate the correlated electronic structures of $\text{La}_3\text{Ni}_2\text{O}_7$ under high pressure. Our calculations show that $\text{La}_3\text{Ni}_2\text{O}_7$ is a multiorbital Hund metal. Both the $3d_{z^2}$ and $3d_{x^2-y^2}$ orbitals of Ni are close to being half filled and contribute the bands crossing the Fermi level. Band renormalization and orbital selective electronic correlation are observed. Through imaginary-time correlation functions, the discovery of high-spin configuration, spin-frozen phase, and spin-orbital separation shows that the system is in a frozen moment phase at high temperatures above 290 K and is a Fermi liquid at low temperatures, which is further confirmed by the calculated spin, orbital, and charge susceptibilities under high temperatures. Our paper uncovers Hundness in $\text{La}_3\text{Ni}_2\text{O}_7$ under high pressure.

DOI: [10.1103/PhysRevB.109.115114](https://doi.org/10.1103/PhysRevB.109.115114)

I. INTRODUCTION

It is well known that a proper description of the electronic correlation effect is the key to understanding unconventional high-temperature (high- T_c) superconductors. Since the discovery of cuprate superconductors [1], numerous scientists have tried to reveal the mechanism of high- T_c superconductivity in the past decades. Although the mechanism of superconductivity in cuprates still remains a puzzle, there are some essential consensuses for cuprates. The parent material of cuprates is considered to be a charge-transfer insulator with strong electronic correlation. Cu atoms have $3d^9$ configuration, and due to the effect of the crystal field $3d_{x^2-y^2}$ orbitals are half filled. By applying hole doping, Cu- $3d_{x^2-y^2}$ orbitals hybridize with O- $2p_x/p_y$ in-plane orbitals, forming the effective singlet band with zero spin moment which is known as the Zhang-Rice singlets [2]. And the superconducting pairing mechanism may be related to the antiferromagnetic spin fluctuations.

Many efforts have been made to search other transition metal compounds analogous to cuprates. As a neighbor of Cu in the periodic table, the Ni element was once considered as a potential candidate to reproduce high- T_c superconductivity. However, no superconductivity trace was observed in hole-doped nickelate $\text{La}_{2-x}\text{Sr}_x\text{NiO}_4$ [3,4], which has the same structure as La_2CuO_4 . In 2019, superconductivity was finally discovered in hole-doped infinite-layer $R\text{NiO}_2$ thin films ($R = \text{La}, \text{Nd}$). With 20% Sr doing, $R_{0.8}\text{Sr}_{0.2}\text{NiO}_2$ shows superconductivity with T_c of 9–15 K [5]. Although the superconducting

T_c is much lower than those of the cuprates, a series of phenomena in nickelates such as self-doping effect [6], absence of long-range magnetic order [7,8], and multiorbital Hund's physics [9] provide some new understandings for unconventional superconductivity.

Very recently, superconductivity was discovered in Ruddlesden-Popper bilayer perovskite nickelate $\text{La}_3\text{Ni}_2\text{O}_7$ with the maximum T_c of about 80 K under pressure [10]. This is undoubtedly a remarkable breakthrough in the field of high- T_c superconductivity since the discovery of cuprates and iron-based superconductors. The x-ray-diffraction patterns show that $\text{La}_3\text{Ni}_2\text{O}_7$ possesses the orthorhombic $Amam$ space group from 1.6 to 10 GPa and transforms to the $Fmmm$ space group above 15 GPa. And the density functional theory (DFT) calculations show that applying pressure could metalize the σ bond formed by Ni and the apical O, which may be a crucial clue for superconductivity. For the electronic structure of high-pressure phase $\text{La}_3\text{Ni}_2\text{O}_7$, many theoretical calculations reveal that e_g orbitals of Ni and $2p$ orbitals of O contribute the bands around the Fermi level [11–19]. $\text{La}_3\text{Ni}_2\text{O}_7$ is experimentally considered to be a paramagnetic metal [20], while a large interorbital hopping between $3d_{z^2}$ and $3d_{x^2-y^2}$ via in-plane $2p_x$ or $2p_y$ orbitals of O is found, which indicates a possible in-plane ferromagnetic tendency in $\text{La}_3\text{Ni}_2\text{O}_7$ [13]. In addition, a bilayer two-orbital model has been constructed by Luo *et al.*, and the spin susceptibility studied by a random-phase approximation method shows that the magnetic signal mostly comes from the d_{z^2} orbitals [11]. Moreover, the superconductivity in $\text{La}_3\text{Ni}_2\text{O}_7$ has been studied. A possible s_{\pm} wave superconducting pairing in $\text{La}_3\text{Ni}_2\text{O}_7$ has been proposed [21]. The model calculations by functional renormalization group method [15] and cluster dynamical mean-field theory [22] both show the pairing tendency of the s_{\pm} wave. Besides, a minimal effective strong-coupling model

*rqhe@ruc.edu.cn

†lihuang.dmf@ruc.edu.cn

‡zlu@ruc.edu.cn

based on local interlayer spin singlets of Ni- $3d_{z^2}$ electrons has been proposed, which highlights the importance of the bilayer structure of $\text{La}_3\text{Ni}_2\text{O}_7$ [23]. As a crucial factor to understanding superconductivity, the electronic correlation in $\text{La}_3\text{Ni}_2\text{O}_7$ is still worth in-depth discussing to figure out the origin of electronic correlation in $\text{La}_3\text{Ni}_2\text{O}_7$.

In this paper, we investigated the electronic structures and correlation of $\text{La}_3\text{Ni}_2\text{O}_7$ by means of density functional theory plus dynamical mean-field theory (DFT+DMFT). We performed the calculations under different finite temperatures. Our results show that $\text{La}_3\text{Ni}_2\text{O}_7$ is a multiorbital Hund metal with orbital selective electronic correlation. The high-spin states and spin-orbital separation revealed by our calculations suggest Hundness rather than Mottness in the system. And the calculated spin, orbital, and charge susceptibilities under high temperatures confirm that the electronic correlation in $\text{La}_3\text{Ni}_2\text{O}_7$ is attributed to Hund's physics. Our paper discovers Hundness in $\text{La}_3\text{Ni}_2\text{O}_7$ under high pressure and provides an understanding to the origin of its electronic correlation.

II. METHOD

We performed DFT+DMFT calculations to study the electronic correlation of $\text{La}_3\text{Ni}_2\text{O}_7$ under different finite temperatures. The DFT parts were done by WIEN2K code and the full-potential linearized augmented plane-wave method was implemented [24]. The optimized unit cell including 12 atoms was used. The cutoff parameter was $R_{\text{MT}}K_{\text{max}} = 7.0$. The muffin-tin radii for La, Ni, and O atoms were fixed to be 2.29, 1.86, and 1.60 bohr, respectively. The generalized gradient approximation with Perdew-Burke-Ernzerhof functional was chosen as the exchange and correlation potential [25]. The k -point mesh for the Brillouin zone integration was $12 \times 12 \times 12$. The EDMFTF software package was used to perform the charge fully self-consistent DFT+DMFT calculations [26]. A good convergence can be achieved within 50 DFT+DMFT cycles. Each DFT+DMFT cycle contained one-shot DMFT calculation and maximum 100 DFT iterations. The convergence criteria for charge and total energy were 10^{-7} eV and 10^{-7} Ry, respectively. We enforced the system to be paramagnetic. Only $3d_{z^2}$ and $3d_{x^2-y^2}$ orbitals of Ni were treated as correlated, considering that t_{2g} orbitals all are fully filled. And a single impurity problem was constructed due to all Ni atoms being equivalent. We chose the Coulomb interaction parameter $U = 5.0$ eV, and the Hund's exchange parameter $J_H = 1.0$ eV, which are typical values for nickelates [9,12,27–33]. And the density-density form of the Coulomb repulsion was used. We used the projectors with an energy window from -10 to 10 eV with respect to the Fermi level to construct the correlated orbitals. The impurity problem was solved by hybridization expansion continuous-time quantum impurity solver [34] with exact double-counting scheme for the self-energy function, which was developed by Haule [35]. The real frequency self-energy function was obtained by analytical continuation with the maximum entropy [36]. Then it was used to calculate the momentum-resolved spectral function and the other related physical quantities. A fine k mesh with 5×10^5 k points is used to obtain spectral functions $A(\omega)$.

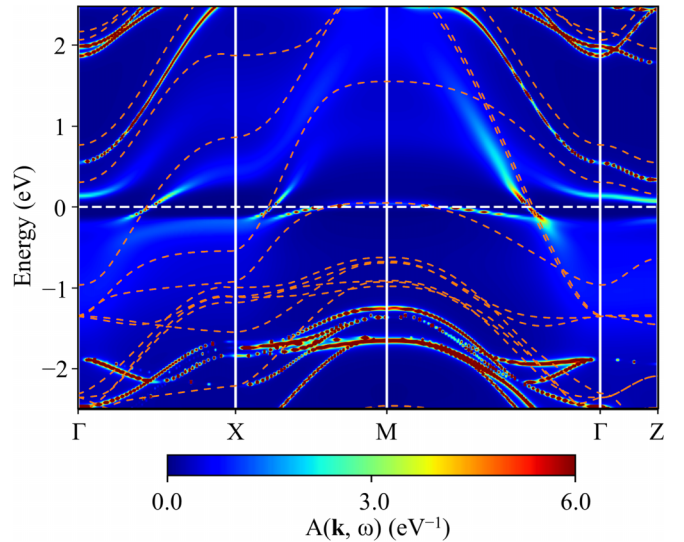


FIG. 1. Momentum-resolved spectral functions $A(\mathbf{k}, \omega)$ obtained by DFT+DMFT calculations at $T = 80$ K. The DFT band structures are plotted with orange dashed lines. The Fermi level is set to zero.

III. RESULTS AND ANALYSIS

A. Band renormalization

Figure 1 shows the DFT band structures and momentum-resolved spectral functions $A(\mathbf{k}, \omega)$ calculated by DFT+DMFT at $T = 80$ K. Both DFT bands and DFT+DMFT spectral functions exhibit that three bands cross the Fermi level. Among them, Ni- $3d_{x^2-y^2}$ and $3d_{z^2}$ orbitals contribute two electron pockets respectively around the Γ and X points and Ni- $3d_{z^2}$ orbitals contribute a hole pocket at the M point. All these electronic bands are consistent with those in the previous reports. The strong interlayer coupling between Ni- $3d_{z^2}$ and apical O- $2p_z$ orbitals leads to the flat bands at the M point split into a bonding state with lower energy and a higher-energy antibonding state. Our DFT+DMFT calculations suggest that those bands around the Fermi level are strongly renormalized due to the electronic correlation. The bandwidth of the Ni- $3d_{z^2}$ bonding state is compressed to 0.3 eV and the antibonding state moves to 0.7 eV above the Fermi level. In addition, we find that the antibonding state locating above the Fermi level at the M point is blurry. This is because a finite temperature makes an electronic incoherent-coherent crossover and a large proportion of electronic excitations are washed out. Similar behavior can be observed in those spectra below the Fermi level. When the temperature is higher, it is expected that the flat band at the M point will become incoherent. But those bands around the Fermi level already show good coherence at $T = 80$ K.

B. Orbital selective electronic correlation

The strong band renormalization suggests electronic correlation in $\text{La}_3\text{Ni}_2\text{O}_7$. It is natural to wonder whether the origin of electronic correlation belongs to Mottness or Hundness. In order to study this problem, in Fig. 2, we show the orbital-resolved spectral functions $A(\omega)$ and imaginary parts of the orbital-dependent self-energy at Matsubara axis $\text{Im}\Sigma(i\omega)$ and

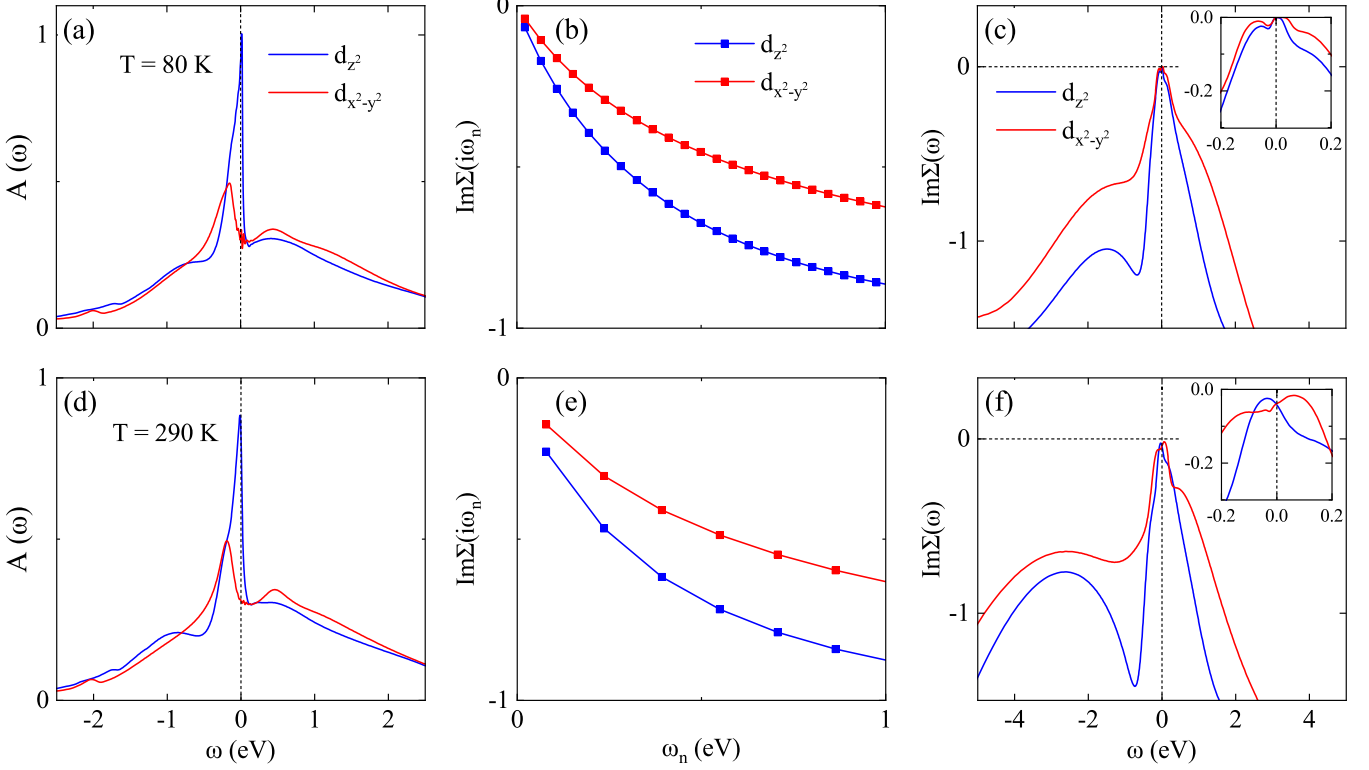


FIG. 2. Orbital-resolved spectral functions $A(\omega)$ and the imaginary parts of self-energy functions at Matsubara axis $\text{Im}\Sigma(i\omega)$ and real axis $\text{Im}\Sigma(\omega)$ obtained by DFT+DMFT calculations at (a–c) $T = 80$ K and (d–f) $T = 290$ K. Insets in (c) and (f): The real axis $\text{Im}\Sigma(\omega)$ around $\omega = 0$.

real axis $\text{Im}\Sigma(\omega)$. As shown in Figs. 2(a) and 2(d), both $3d_{z^2}$ and $3d_{x^2-y^2}$ orbitals appear around the Fermi level, which indicates a multiorbital metallic behavior. For each orbital, a narrow quasiparticle coherence peak appears near the Fermi level. As the temperature decreases from 290 to 80 K, these coherence peaks become sharper, which is consistent to the trend forming a coherent Fermi liquid at lower temperatures [37]. This peak for the $3d_{z^2}$ orbital is much higher than that of the $3d_{x^2-y^2}$ orbital because, as shown in Fig. 1, the band for the $3d_{z^2}$ orbital is very flat.

Then, we show the imaginary parts of self-energy functions at the Matsubara axis $\text{Im}\Sigma(i\omega)$ in Figs. 2(b) and 2(e). Orbital selective electronic correlation is observed at both 80 and 290 K. Furthermore, we also show the imaginary parts of real axis self-energy $\text{Im}\Sigma(\omega)$ in Figs. 2(c) and 2(f) to roughly describe a likely phase transition in $\text{La}_3\text{Ni}_2\text{O}_7$. At high temperature if the system is in a frozen moment phase, electrons suffering scattering from the moments are expected so that $\text{Im}\Sigma(\omega = 0)$ is equal to a finite value Γ , which is corresponding to the intercept $\text{Im}\Sigma(i\omega \rightarrow 0) = \Gamma \text{sgn}(\omega_n)$ [38,39]. In contrast, the Fermi liquid behavior may be expected at lower temperatures with a linearly vanishing self-energy [$\text{Im}\Sigma(i\omega) \sim \omega$] at small ω . Our calculated imaginary parts of self-energy functions at real axis $\text{Im}\Sigma(\omega)$ show such a trend. An intercept $\text{Im}\Sigma(\omega = 0) = \Gamma$ is observed at $T = 290$ K but disappears at $T = 80$ K. This finding suggests that the crossover from the frozen moment phase [37,38] to the Fermi liquid phase may happen around 80 K.

In order to further characterize the orbital selective electronic correlation in $\text{La}_3\text{Ni}_2\text{O}_7$, we list the orbital mass

enhancement in Table I, which is a key factor to characterize the band renormalization, as well as the electronic correlation. The mass enhancement is defined as

$$m^*/m = Z^{-1} = 1 - \left. \frac{\partial \text{Im}\Sigma(i\omega)}{\partial \omega} \right|_{\omega \rightarrow 0}. \quad (1)$$

Z is the renormalization factor, which can be estimated from self-energy functions at the Matsubara axis. We find a mass enhancement difference of 2.5 and 2.0 for the $3d_{z^2}$ and $3d_{x^2-y^2}$ orbitals at $T = 290$ K, respectively. Such a difference becomes more significant when temperature is lower, with a stronger mass enhancement of 3.4 for $3d_{z^2}$ and weaker mass enhancement of 2.5 for $3d_{x^2-y^2}$ at $T = 80$ K. The mass enhancement confirms the strong renormalization of band structures in Fig. 1. And the difference of mass enhancement suggests the orbital selective electronic correlation in $\text{La}_3\text{Ni}_2\text{O}_7$. Furthermore, we show the local occupancy number N_{e_g} for the e_g orbitals of Ni. According to the nominal electron

TABLE I. The mass enhancement m^*/m and the local occupancy number N_{e_g} for the e_g orbitals of Ni obtained by DFT+DMFT calculations under different temperatures.

Temperature (K)		80	150	220	290
m^*/m	$3d_{z^2}$	3.394	3.019	2.736	2.516
	$3d_{x^2-y^2}$	2.529	2.333	2.157	2.015
N_{e_g}	$3d_{z^2}$	1.140	1.139	1.139	1.139
	$3d_{x^2-y^2}$	1.056	1.056	1.056	1.056

TABLE II. Weights of the Ni e_g orbital local multiplets obtained by DFT+DMFT calculations at temperature T of 80 and 290 K, respectively.

N_Γ	0	1	2	2	3	4
S_z	0	1/2	0	1	1/2	0
P_Γ (80 K)	0.40%	12.41%	23.85%	32.94%	28.10%	2.30%
P_Γ (290 K)	0.39%	12.36%	23.62%	33.28%	28.06%	2.29%

count, a $\text{Ni}^{2.5+}$ cation with $3d^{7.5}$ occupancy is expected in $\text{La}_3\text{Ni}_2\text{O}_7$. Considering the crystal field of the Ni-O octahedra, t_{2g} orbitals are fully filled, and the occupancy number N_{e_g} is thus about 1.5. However, as shown by our DFT+DMFT calculation results, a larger occupancy of 2.2 is found in the e_g orbitals. This result is consistent with a previous DFT+DMFT study [17]. At other different temperature conditions, the occupancy of $3d_{z^2}$ and $3d_{x^2-y^2}$ orbitals is close to being half filled. Both orbital selective electronic correlation and near half-filled occupancy in $3d_{z^2}$ and $3d_{x^2-y^2}$ orbitals indicate possible characteristic multiorbital Hund's metal behaviors in $\text{La}_3\text{Ni}_2\text{O}_7$.

C. Hundness from high-spin states

Here, we survey the local spin multiplets to demonstrate the Hund correlation in $\text{La}_3\text{Ni}_2\text{O}_7$. In those strongly correlated materials that exhibit Hundness, the high-spin states are usually favored [40,41]. In Table II, we list the probability P_Γ of all local spin multiplets for given atomic configurations $|\Gamma\rangle$, which are labeled by some good quantum numbers, such as total spin S_z and total occupancy N_Γ . For the e_g orbitals of Ni, up to four electrons are allowed to be filled in. Among these atomic configurations under $T = 290$ K, the high-spin state $S_z = 1$ only exists when total occupancy $N_{e_g} = 2$, which accounts for approximately 33.28%, while the low-spin state with $N_{e_g} = 2$, $S_z = 0$ possesses a smaller percentage of 23.62%. Such a difference indicates the existence of Hund interorbital correlation in $\text{La}_3\text{Ni}_2\text{O}_7$. Additionally, we find the charge fluctuations with 0.39, 12.36, 28.06, and 2.29% multiplets in $N = 0, 1, 3$, and 4, respectively. Thus, the averaged occupancy of the e_g orbitals $\langle N_{e_g} \rangle \equiv \sum_\Gamma N_\Gamma P_\Gamma$ is about 2.19, which is consistent with N_{e_g} in Table I and larger than the nominal occupancy of 1.5 with $\text{Ni}^{2.5+}$. And the atomic configurations under $T = 80$ K also show that the high-spin state possesses a larger percentage. All these results suggest electronic correlation of Hundness in $\text{La}_3\text{Ni}_2\text{O}_7$.

D. Hundness from imaginary-time correlation

Then, we study the spin-spin correlation function $C_{ss}(\tau) = \langle S_z(\tau)S_z(0) \rangle$ and orbital-orbital correlation function $C_{oo}(\tau) = \langle O(\tau)O(0) \rangle$ obtained by DFT+DMFT calculations at different temperatures, where S_z is the total spin, and O means the difference between the orbital occupancy numbers $n(d_{x^2-y^2}) - n(d_{z^2})$. In Fig. 3(a), first, we see that at a finite temperature of $T = 1100$ K, $C_{ss}(\tau)$ decays much slower than $C_{oo}(\tau)$ with imaginary time, which indicates spin-orbital separation [40,42]. In Fig. 3(b), we exhibit a series of calculated $C_{ss}(\tau)$ under different temperatures. A large finite value of

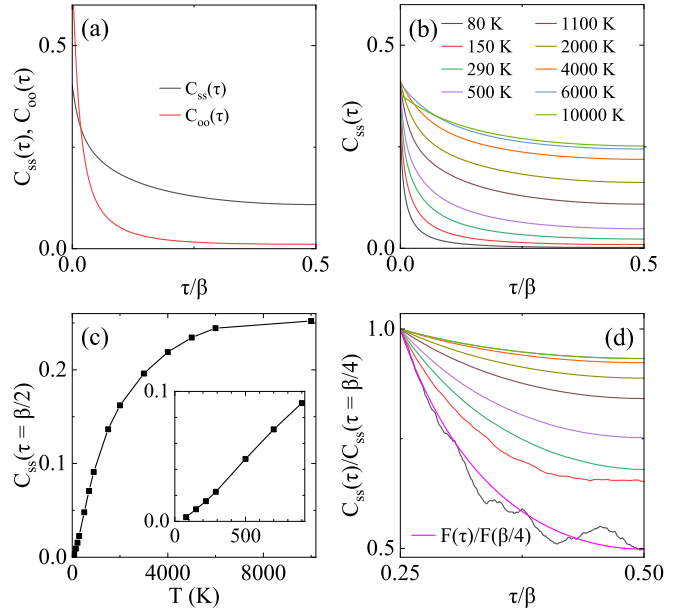


FIG. 3. (a) Imaginary-time spin-spin correlation functions $C_{ss}(\tau)$ and orbital-orbital correlation functions $C_{oo}(\tau)$ obtained by DFT+DMFT calculations at $T = 1100$ K. (b) Imaginary-time spin-spin correlation functions $C_{ss}(\tau)$ at different temperatures. (c) $C_{ss}(\tau = \beta/2)$ plotted as a function of temperature. (d) Calculated $C_{ss}(\tau = \beta/4)/C_{ss}(\tau = \beta/4)$ at different temperatures, where $F(t) = [T / \sin(\pi t / \beta)]^2$.

$C_{ss}(\tau = \beta/2)$ is observed above $T = 1100$ K, which suggests that the system is in spin frozen phase [38,40]. It should be noted that here we only want to simulate the behaviors of the electronic system under high-temperature scales; such an extremely high temperature is not actually applied to the real crystal system, but just applied to electrons like external field to detect the corresponding responses of the electrons. Both spin-orbital separation and spin frozen phase are key signatures of Hundness, which have been observed in some typical Hund metals such as Sr_2RuO_4 [37]. In Fig. 3(c), a $C_{ss}(\tau = \beta/2) \sim T$ scaling is found above $T = 290$ K and a $C_{ss}(\tau = \beta/2) \sim T^2$ behavior is found at low temperatures. Such scaling behaviors are also found in a three-orbital model studied by Werner *et al.* [38]. $C_{ss}(\tau = \beta/2) \sim T$ scaling is expected to emerge near the phase transition point from a frozen moment phase to a Fermi liquid phase [38]. Besides, at a low-temperature Fermi liquid phase, $C_{ss}(\tau) \sim F(\tau) = [T / \sin(\pi \tau T)]^2$ for imaginary times τ sufficiently far from either $\tau = 0$ or β and $C_{ss}(\tau) \sim T^2$ at $\tau = \beta/2$. In Fig. 4(d), $C_{ss}(\tau = \beta/2)$ at $T = 80$ K shows such a behavior, indicating that the system is in a Fermi liquid phase at low temperatures.

E. Hundness from susceptibilities

To further elucidate the origin of electronic correlation in $\text{La}_3\text{Ni}_2\text{O}_7$, we now study the static local susceptibilities under different temperatures. First of all, four temperature scales are identified, which characterize the onset and completion of screening of the orbital and spin degrees of freedom as the temperature is lowered. $T_{\text{orbital}}^{\text{onset}}$ and $T_{\text{spin}}^{\text{onset}}$ mark the onset temperatures of the screening for orbital and spin degrees

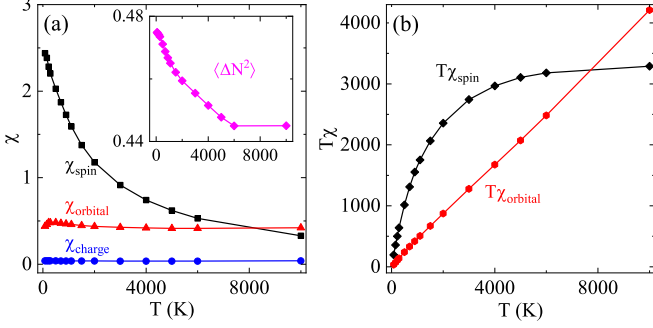


FIG. 4. (a) Static local susceptibilities χ for spin, orbital, and charge obtained by DFT+DMFT calculations under different finite temperatures. (b) $T\chi_{\text{spin}}$ and $T\chi_{\text{orbital}}$ plotted as functions of temperature. Inset in (a): Local charge fluctuation $\langle \Delta N^2 \rangle$.

of freedom, respectively. $T_{\text{orbital}}^{\text{cmp}}$ and $T_{\text{spin}}^{\text{cmp}}$ are defined as the completion temperatures of the screening [37]. When the temperature is lower than T^{onset} , the static local orbital and spin susceptibilities χ_{orbital} and χ_{spin} deviate from the Curie-Weiss behavior $\chi \sim \frac{1}{T}$. Below T^{cmp} these susceptibilities become constant, which is known as the Pauli behavior. In a Mott system, the screening of orbitals and spins begins almost simultaneously, as well as the completion ($T_{\text{orbital}}^{\text{onset}} \sim T_{\text{spin}}^{\text{onset}}$). In contrast, a Hundness system possesses a smaller value of U and a larger value of J_H , which causes the screening of orbitals to start before the spin screening at a much higher temperature ($T_{\text{orbital}}^{\text{onset}} \gg T_{\text{spin}}^{\text{onset}}$). This is the so-called spin-orbital separation. Usually, such a behavior in a Hundness system features a broader temperature window than in a Mott system. And in such a spin-orbital separation phase, the completely screened orbital degree of freedom shows a Pauli behavior while χ_{spin} deviates from a Curie behavior. Meanwhile, a non-Fermi-liquid behavior is observed in this phase till both the spin and orbital screenings complete. This is a key signature to identify the Hund electronic correlation in correlated materials.

In Fig. 4, we show the static local susceptibilities of spin, orbital, and charge plotted as functions of temperature. The χ_{spin} , χ_{orbital} , and χ_{charge} are defined as

$$\chi_{\text{spin}} = \int_0^\beta \langle S_z(\tau) S_z(0) \rangle d\tau, \quad (2)$$

$$\chi_{\text{orbital}} = \int_0^\beta \langle O(\tau) O(0) \rangle d\tau - \beta \langle O \rangle^2, \quad (3)$$

$$\chi_{\text{charge}} = \int_0^\beta \langle N(\tau) N(0) \rangle d\tau - \beta \langle N \rangle^2, \quad (4)$$

where $O = n(d_{x^2-y^2}) - n(d_{z^2})$ is the orbital occupancy difference, and N is the total occupancy of the two e_g orbitals. From a very high temperature of $T = 10000$ K, we find that χ_{orbital} are almost unchanged when lowering the temperature. The unchanged χ_{orbital} strongly suggests that the screening of orbitals has completed at an extremely higher temperature than $T = 10000$ K. However, χ_{spin} and χ_{orbital} show obviously different behaviors when changing temperature. As the temperature decreases, χ_{spin} generally shows an increasing trend, while χ_{orbital} remains constant. We then display the $T\chi_{\text{spin}}$ and $T\chi_{\text{orbital}}$ curves versus temperature in Fig. 4(b).

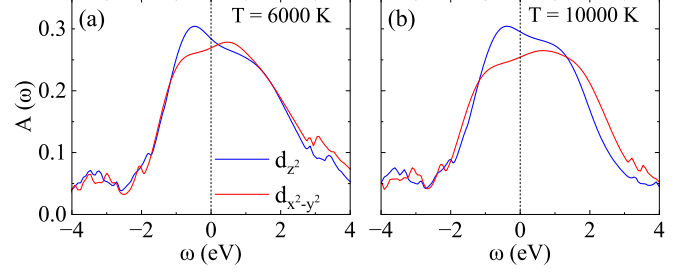


FIG. 5. Orbital-resolved spectral functions $A(\omega)$ obtained by DFT+DMFT calculations for (a) $T = 6000$ K and (b) $T = 10000$ K. The blue and red lines represent the $3d_{z^2}$ and $3d_{x^2-y^2}$ orbitals of Ni, respectively.

We see that the variation of $T\chi_{\text{orbital}}$ keeps a linear behavior, which deviates from the Curie-Weiss law. In contrast, $T\chi_{\text{spin}}$ shows a Curie behavior above $T = 5000$ K, which is approximately constant. When the temperature is lower than $T = 5000$ K, the Curie behavior is broken, indicating the onset of spin screening. And a broad non-Fermi-liquid phase appears, which is corresponding to the spin-orbital separation. Within the process of spin screening, $C_{ss}(\tau)$ decays as the temperature decreases [Fig. 3(b)]. And a tendency towards a constant for χ_{spin} begins to be observed at $T = 80$ K, which suggests that the spin screening completes. This finding is consistent with our previous results, for example, the zero intercept of $\text{Im}\Sigma(\omega = 0)$ and the scaling behavior of $C_{oo}(\tau = \beta/2) \sim T^2$ at $T = 80$ K, showing the low-temperature Fermi liquid phase.

F. Absence of Mottness

In order to check the Mott electronic correlation in $\text{La}_3\text{Ni}_2\text{O}_7$, we exhibit the orbital-resolved spectral functions $A(\omega)$ at larger temperatures, where the spin screening has not started. For instance, in V_2O_3 , which is an archetypal Mott correlated metal [37], before the onset of spin screening, a pseudogap feature is observed. But no pseudogap is observed in $\text{La}_3\text{Ni}_2\text{O}_7$ under $T = 6000$ and 10000 K (Fig. 5). In addition, we also find that both the local charge fluctuation $\langle \Delta N^2 \rangle = \langle N^2 \rangle - \langle N \rangle^2$ and χ_{charge} are almost unchanged when the temperature is lower [Fig. 4(a)], while in a Mottness system $\langle \Delta N^2 \rangle$ should have an obvious temperature dependence, manifesting delocalization of electrons [37]. All these findings suggest that the electronic correlation in $\text{La}_3\text{Ni}_2\text{O}_7$ is attributed to Hund's physics.

IV. DISCUSSION AND CONCLUSION

Hund's coupling plays a crucial role in electronic structures, magnetism, and superconducting pairing mechanisms in $\text{La}_3\text{Ni}_2\text{O}_7$. The Hund electronic correlation brings strong band normalization and orbital-selective electronic correlation, which have been widely reported in other DFT+DMFT electronic structure studies [12, 17, 18]. Although a long-range magnetic order has not been observed in $\text{La}_3\text{Ni}_2\text{O}_7$, some theoretical model studies suggest that the half-filled d_{z^2} orbitals of two layers can couple via the interlayer antiferromagnetic superexchange interaction. This superexchange interaction

can be transmitted to the $d_{x^2-y^2}$ orbitals by Hund's coupling [22,43,44]. As for the superconducting mechanism, an s_{\pm} -wave pairing is favored. And the superconducting critical energy scale increases with J_H , until a spin density wave begins to win for larger U and J_H [21]. In the doped case, the superconducting phase diagram becomes richer, and a time-reversal symmetry breaking $s + id$ -wave pairing emerges [43], where Hund's coupling still plays an important role. There are numerous reports emphasizing that Hund's physics has a crucial effect on the physical properties of $\text{La}_3\text{Ni}_2\text{O}_7$. Our paper has exactly revealed qualitatively the Hund electronic correlation in $\text{La}_3\text{Ni}_2\text{O}_7$ via DFT+DMFT calculations.

In summary, we have studied the electronic structures and correlation of $\text{La}_3\text{Ni}_2\text{O}_7$ via DFT+DMFT calculations. The momentum-resolved spectral functions $A(\mathbf{k}, \omega)$ show that $\text{La}_3\text{Ni}_2\text{O}_7$ is a multiorbital metal. The $3d_{z^2}$ and $3d_{x^2-y^2}$ orbitals of Ni contribute those bands crossing the Fermi level. The electronic correlation leads to a strong band renormalization, where the band width of the bonding state band at the M point is reduced remarkably. The orbital-resolved spectral functions $A(\omega)$ show sharp quasiparticle coherence peaks around the Fermi level. The mass enhancement m^*/m derived from the self-energy functions at the Matsubara axis reveals the orbital selective electronic correlation. The electronic correlation of the $3d_{z^2}$ orbital is stronger than that of the $3d_{x^2-y^2}$

orbital. At $T = 80$ K, the mass enhancements of the $3d_{z^2}$ and $3d_{x^2-y^2}$ orbitals are about 3.4 and 2.5, respectively. A higher percentage of high-spin state suggests the existence of interorbital Hund electronic correlation within the e_g orbitals of Ni. Moreover, the calculated spin-spin and orbital-orbital correlation functions show spin-orbital separation and frozen moments at high temperatures. The scaling behavior of the spin-spin correlation functions indicates that $\text{La}_3\text{Ni}_2\text{O}_7$ is in a spin-frozen phase at high temperatures ($T > 290$ K) or in a Fermi liquid phase at low temperatures. The calculated static local spin, orbital, and charge susceptibilities under high temperatures also show signatures of Hundness. All these results show that $\text{La}_3\text{Ni}_2\text{O}_7$ is a multiorbital Hund's metal. Our DFT+DMFT calculations uncover the Hund electronic correlation in $\text{La}_3\text{Ni}_2\text{O}_7$ and also provide a perspective to understand the origin of electronic correlation in correlated materials.

ACKNOWLEDGMENTS

This work was supported by the National Natural Science Foundation of China (Grant No. 11934020). L.H. was also supported by the CAEP Foundation (Grant No. CX20210033). Computational resources were provided by the Physical Laboratory of High Performance Computing at Renmin University of China.

-
- [1] J. G. Bednorz and K. A. Müller, Possible high- T_c superconductivity in the Ba-La-Cu-O system, *Z. Phys. B* **64**, 189 (1986).
- [2] F. C. Zhang and T. M. Rice, Effective Hamiltonian for the superconducting Cu oxides, *Phys. Rev. B* **37**, 3759 (1988).
- [3] C. H. Chen, S.-W. Cheong, and A. S. Cooper, Charge modulations in $\text{La}_{2-x}\text{Sr}_x\text{NiO}_{4+y}$: Ordering of polarons, *Phys. Rev. Lett.* **71**, 2461 (1993).
- [4] S.-W. Cheong, H. Y. Hwang, C. H. Chen, B. Batlogg, L. W. Rupp, and S. A. Carter, Charge-ordered states in $(\text{La}, \text{Sr})_2\text{NiO}_4$ for hole concentrations $n_h = 1/3$ and $1/2$, *Phys. Rev. B* **49**, 7088 (1994).
- [5] D. Li, K. Lee, B. Y. Wang, M. Osada, S. Crossley, H. R. Lee, Y. Cui, Y. Hikita, and H. Y. Hwang, Superconductivity in an infinite-layer nickelate, *Nature (London)* **572**, 624 (2019).
- [6] Q. Gu and H.-H. Wen, Superconductivity in nickel-based 112 systems, *The Innovation* **3**, 100202 (2022).
- [7] M. A. Hayward, M. A. Green, M. J. Rosseinsky, and J. Sloan, Sodium hydride as a powerful reducing agent for topotactic oxide deintercalation: Synthesis and characterization of the nickel(I) oxide LaNiO_2 , *J. Am. Chem. Soc.* **121**, 8843 (1999).
- [8] M. A. Hayward and M. J. Rosseinsky, Synthesis of the infinite layer Ni(I) phase NdNiO_{2+x} by low temperature reduction of NdNiO_3 with sodium hydride, *Solid State Sci.* **5**, 839 (2003).
- [9] Y. Wang, C.-J. Kang, H. Miao, and G. Kotliar, Hund's metal physics: From SrNiO_2 to LaNiO_2 , *Phys. Rev. B* **102**, 161118(R) (2020).
- [10] H. Sun, M. Huo, X. Hu, J. Li, Z. Liu, Y. Han, L. Tang, Z. Mao, P. Yang, B. Wang, J. Cheng, D.-X. Yao, G.-M. Zhang, and M. Wang, Signatures of superconductivity near 80 K in a nickelate under high pressure, *Nature (London)* **621**, 493 (2023).
- [11] Z. Luo, X. Hu, M. Wang, W. Wú, and D.-X. Yao, Bilayer two-orbital model of $\text{La}_3\text{Ni}_2\text{O}_7$ under pressure, *Phys. Rev. Lett.* **131**, 126001 (2023).
- [12] F. Lechermann, J. Gondolf, S. Bötzel, and I. M. Eremin, Electronic correlations and superconducting instability in $\text{La}_3\text{Ni}_2\text{O}_7$ under high pressure, *Phys. Rev. B* **108**, L201121 (2023).
- [13] Y. Zhang, L.-F. Lin, A. Moreo, and E. Dagotto, Electronic structure, dimer physics, orbital-selective behavior, and magnetic tendencies in the bilayer nickelate superconductor $\text{La}_3\text{Ni}_2\text{O}_7$ under pressure, *Phys. Rev. B* **108**, L180510 (2023).
- [14] H. Sakakibara, N. Kitamine, M. Ochi, and K. Kuroki, Possible high T_c superconductivity in $\text{La}_3\text{Ni}_2\text{O}_7$ under high pressure through manifestation of a nearly-half-filled bilayer Hubbard model, *Phys. Rev. Lett.* **132**, 106002 (2024).
- [15] Y. Gu, C. Le, Z. Yang, X. Wu, and J. Hu, Effective model and pairing tendency in bilayer Ni-based superconductor $\text{La}_3\text{Ni}_2\text{O}_7$, *arXiv:2306.07275*.
- [16] V. Christiansson, F. Petocchi, and P. Werner, Correlated electronic structure of $\text{La}_3\text{Ni}_2\text{O}_7$ under pressure, *Phys. Rev. Lett.* **131**, 206501 (2023).
- [17] D. A. Shilenko and I. V. Leonov, Correlated electronic structure, orbital-selective behavior, and magnetic correlations in double-layer $\text{La}_3\text{Ni}_2\text{O}_7$ under pressure, *Phys. Rev. B* **108**, 125105 (2023).
- [18] Y. Cao and Y.-F. Yang, Flat bands promoted by Hund's rule coupling in the candidate double-layer high-temperature superconductor $\text{La}_3\text{Ni}_2\text{O}_7$ under high pressure, *Phys. Rev. B* **109**, L081105 (2024).
- [19] X. Chen, P. Jiang, J. Li, Z. Zhong, and Y. Lu, Critical charge and spin instabilities in superconducting $\text{La}_3\text{Ni}_2\text{O}_7$, *arXiv:2307.07154*.

- [20] Z. Liu, H. Sun, M. Huo, X. Ma, Y. Ji, E. Yi, L. Li, H. Liu, J. Yu, Z. Zhang, Z. Chen, F. Liang, H. Dong, H. Guo, D. Zhong, B. Shen, S. Li, and M. Wang, Evidence for charge and spin density waves in single crystals of $\text{La}_3\text{Ni}_2\text{O}_7$ and $\text{La}_3\text{Ni}_2\text{O}_6$, *Sci. China Phys. Mech. Astron.* **66**, 217411 (2023).
- [21] Q.-G. Yang, D. Wang, and Q.-H. Wang, Possible s_{\pm} -wave superconductivity in $\text{La}_3\text{Ni}_2\text{O}_7$, *Phys. Rev. B* **108**, L140505 (2023).
- [22] Y.-H. Tian, Y. Chen, J.-M. Wang, R.-Q. He, and Z.-Y. Lu, Correlation effects and concomitant two-orbital s_{\pm} -wave superconductivity in $\text{La}_3\text{Ni}_2\text{O}_7$ under high pressure, [arXiv:2308.09698](https://arxiv.org/abs/2308.09698).
- [23] Y.-F. Yang, G.-M. Zhang, and F.-C. Zhang, Interlayer valence bonds and two-component theory for high- T_c superconductivity of $\text{La}_3\text{Ni}_2\text{O}_7$ under pressure, *Phys. Rev. B* **108**, L201108 (2023).
- [24] P. Blaha, K. Schwarz, F. Tran, R. Laskowski, G. K. H. Madsen, and L. D. Marks, WIEN2k: An APW+lo program for calculating the properties of solids, *J. Chem. Phys.* **152**, 074101 (2020).
- [25] J. P. Perdew, K. Burke, and M. Ernzerhof, Generalized gradient approximation made simple, *Phys. Rev. Lett.* **77**, 3865 (1996).
- [26] K. Haule, C.-H. Yee, and K. Kim, Dynamical mean-field theory within the full-potential methods: Electronic structure of CeIrIn_5 , CeCoIn_5 , and CeRhIn_5 , *Phys. Rev. B* **81**, 195107 (2010).
- [27] H. Sakakibara, H. Usui, K. Suzuki, T. Kotani, H. Aoki, and K. Kuroki, Model construction and a possibility of cupratelike pairing in a new d^9 nickelate superconductor $(\text{Nd}, \text{Sr})\text{NiO}_2$, *Phys. Rev. Lett.* **125**, 077003 (2020).
- [28] I. Leonov, S. L. Skornyakov, and S. Y. Savrasov, Lifshitz transition and frustration of magnetic moments in infinite-layer NdNiO_2 upon hole doping, *Phys. Rev. B* **101**, 241108(R) (2020).
- [29] F. Lechermann, Multiorbital processes rule the $\text{Nd}_{1-x}\text{Sr}_x\text{NiO}_2$ normal state, *Phys. Rev. X* **10**, 041002 (2020).
- [30] F. Lechermann, Doping-dependent character and possible magnetic ordering of NdNiO_2 , *Phys. Rev. Mater.* **5**, 044803 (2021).
- [31] F. Lechermann, Assessing the correlated electronic structure of lanthanum nickelates, *Electron. Struct.* **4**, 015005 (2022).
- [32] F. Lechermann, Late transition metal oxides with infinite-layer structure: Nickelates versus cuprates, *Phys. Rev. B* **101**, 081110(R) (2020).
- [33] F. Lechermann, Emergent flat-band physics in $d^{9-\delta}$ multilayer nickelates, *Phys. Rev. B* **105**, 155109 (2022).
- [34] K. Haule, Quantum Monte Carlo impurity solver for cluster dynamical mean-field theory and electronic structure calculations with adjustable cluster base, *Phys. Rev. B* **75**, 155113 (2007).
- [35] K. Haule, Exact double counting in combining the dynamical mean field theory and the density functional theory, *Phys. Rev. Lett.* **115**, 196403 (2015).
- [36] M. Jarrell and J. E. Gubernatis, Bayesian inference and the analytic continuation of imaginary-time quantum Monte Carlo data, *Phys. Rep.* **269**, 133 (1996).
- [37] X. Deng, K. M. Stadler, K. Hauler, A. Weichselbaum, J. von Delft, and G. Kotliar, Signatures of Mottness and Hundness in archetypal correlated metals, *Nat. Commun.* **10**, 2721 (2019).
- [38] P. Werner, E. Gull, M. Troyer, and A. J. Millis, Spin freezing transition and non-Fermi-liquid self-energy in a three-orbital model, *Phys. Rev. Lett.* **101**, 166405 (2008).
- [39] G. R. Stewart, Non-Fermi-liquid behavior in d - and f -electron metals, *Rev. Mod. Phys.* **73**, 797 (2001).
- [40] K. Stadler, G. Kotliar, A. Weichselbaum, and J. von Delft, Hundness versus Mottness in a three-band Hubbard-Hund model: On the origin of strong correlations in Hund metals, *Ann. Phys. (NY)* **405**, 365 (2019).
- [41] Z. P. Yin, K. Haule, and G. Kotliar, Kinetic frustration and the nature of the magnetic and paramagnetic states in iron pnictides and iron chalcogenides, *Nat. Mater.* **10**, 932 (2011).
- [42] L. Huang and H. Lu, Signatures of Hundness in kagome metals, *Phys. Rev. B* **102**, 125130 (2020).
- [43] C. Lu, Z. Pan, F. Yang, and C. Wu, Interlayer coupling driven high-temperature superconductivity in $\text{La}_3\text{Ni}_2\text{O}_7$ under pressure, [arXiv:2307.14965](https://arxiv.org/abs/2307.14965).
- [44] H. Oh and Y.-H. Zhang, Type-II $t - J$ model and shared superexchange coupling from Hund's rule in superconducting $\text{La}_3\text{Ni}_2\text{O}_7$, *Phys. Rev. B* **108**, 174511 (2023).